Local Charge and Spin Currents in Magnetothermal Landscapes

Mathias Weiler,[1] Matthias Althammer,[1] Franz D. Czeschka,[1] Hans Huebl,[1] Martin S. Wagner,[1] Matthias Opel,[1] Inga-Mareen Imort,[2] Günter Reiss,[2] Andy Thomas,[2] Rudolf Gross,[1,3] and Sebastian T. B. Goennenwein[1,*]

[1]*Walther-Meißner-Institut, Bayerische Akademie der Wissenschaften, 85748 Garching, Germany*
[2]*Fakultät für Physik, Universität Bielefeld, 33615 Bielefeld, Germany*
[3]*Physik-Department, Technische Universität München, 85748 Garching, Germany*
(Received 18 October 2011; published 5 March 2012)

A scannable laser beam is used to generate local thermal gradients in metallic (Co_2FeAl) or insulating ($Y_3Fe_5O_{12}$) ferromagnetic thin films. We study the resulting local charge and spin currents that arise due to the anomalous Nernst effect (ANE) and the spin Seebeck effect (SSE), respectively. In the local ANE experiments, we detect the voltage in the Co_2FeAl thin film plane as a function of the laser-spot position and external magnetic field magnitude and orientation. The local SSE effect is detected in a similar fashion by exploiting the inverse spin Hall effect in a Pt layer deposited on top of the $Y_3Fe_5O_{12}$. Our findings establish local thermal spin and charge current generation as well as spin caloritronic domain imaging.

DOI: 10.1103/PhysRevLett.108.106602 PACS numbers: 72.20.Pa, 72.25.Mk, 75.70.Kw

Spin caloritronic effects have been extensively studied using integral (homogeneous) thermal gradients [1,2]. In ferromagnetic conductors exposed to a thermal gradient in the Nernst geometry, one observes the anomalous Nernst effect (ANE), which describes the occurrence of an electric field $\boldsymbol{E}_{\mathrm{ANE}} \propto -\boldsymbol{M} \times \nabla T$, perpendicular to both the temperature gradient ∇T and the magnetization $\boldsymbol{M}$. The anomalous Nernst effect has been studied in a variety of ferromagnetic thin film metals [3,4], oxides [4,5], spinels [4,6,7], and diluted magnetic semiconductors [8]. In analogy to charge-based caloritronic effects, the recently discovered spin Seebeck effect (SSE) [9] describes the generation of a spin current $\boldsymbol{J}_s$ parallel to an applied temperature gradient ∇T in ferromagnetic materials. $\boldsymbol{J}_s$ can be detected all electrically by exploiting the inverse spin Hall effect (ISHE) [10,11] in a normal metal deposited on top of the ferromagnet. In the longitudinal spin Seebeck configuration [12], ∇T is applied along the FM/N hybrid normal, resulting in an electric field $\boldsymbol{E}_{\mathrm{ISHE}} \propto \boldsymbol{J}_s \times \boldsymbol{\sigma}$. Here, $\boldsymbol{\sigma} \parallel \boldsymbol{M}$ is the spin polarization, such that the symmetry of the SSE is identical to the ANE with respect to $\boldsymbol{M}$ and ∇T. Spin Seebeck measurements have been carried out in ferromagnetic metals [9,13], diluted magnetic semiconductors [14], and magnetic insulators [15]. The interplay of spins and temperature leads to further intriguing effects such as the spin Peltier effect [16,17], thermal spin torque [18,19], or thermally driven spin injection [20,21]. However, in all spin caloritronic experiments mentioned above, homogeneous temperature gradients were applied. In order to establish the interplay between temperature gradients and spin degrees of freedom also on the length scale of the magnetic microstructure, temperature gradients changing on such length scales are mandatory. Here, we therefore use a focused, scanning laser beam to generate a local temperature gradient perpendicular to a thin film sample plane and perform a spatially resolved study of the resulting spin caloritronic effects. Our findings demonstrate the generation of local, bipolar, magnetically controllable electric fields and spin currents. This opens the path for spatially resolved spin caloritronic experiments at, e.g., magnetic domain walls, grain boundaries, interfaces, or defects.

In these spatially resolved experiments, the local anomalous Nernst effect in a conductive ferromagnetic thin film results in an electric field

$$\boldsymbol{E}_{\mathrm{ANE}}(x, y) = -N\mu_0 \boldsymbol{M}(x, y) \times \nabla T(x, y), \tag{1}$$

at position (x, y) with the Nernst coefficient N. In samples consisting of a ferromagnetic-insulator–normal-metal bilayer exposed to a local temperature gradient, the spin Seebeck and inverse spin Hall effect yield a local electric field

$$\boldsymbol{E}_{\mathrm{ISHE}}(x, y) = -S\boldsymbol{\sigma}(x, y) \times \nabla T(x, y), \tag{2}$$

defined analogous to the integral expression found in Ref. [14] with the phenomenological spin Seebeck coefficient S and the spin polarization vector $\boldsymbol{\sigma} = \boldsymbol{M}/M_s$, with the saturation magnetization M_s. Comparing Eq. (1) and Eq. (2), it is evident that $\boldsymbol{E}_{\mathrm{ANE}}$ and $\boldsymbol{E}_{\mathrm{ISHE}}$ bear identical symmetry. Hence, both $\boldsymbol{E}_{\mathrm{ANE}}(x, y)$ and $\boldsymbol{E}_{\mathrm{ISHE}}(x, y)$ can be detected in an identical fashion, enabling a spatially resolved investigation of charge and spin currents in a magnetothermal experiment. It is important to note that $\boldsymbol{E}_{\mathrm{ANE}}(x, y)$ and $\boldsymbol{E}_{\mathrm{ISHE}}(x, y)$ are local electric fields, determined by the magnetic properties and temperature gradient at position (x, y). In conductive ferromagnets with $N \neq 0$, a spatially confined $\nabla T(x, y)$ will thus evoke a local $\boldsymbol{E}_{\mathrm{ANE}}(x, y)$. Its magnitude and polarity are controllable *in situ* by manipulating $\boldsymbol{M}(x, y)$. Vice versa, $\boldsymbol{E}_{\mathrm{ANE}}(x, y)$ can be used to electrically readout the magnetization

 © 2012 American Physical Society

$\boldsymbol{M}(x, y)$ with full 360° confidence, i.e., to electrically image the magnetic microstructure by scanning $\nabla T(x, y)$ across the sample. Identical considerations apply in magnetic-insulator–normal-metal bilayers where $\boldsymbol{E}_{\mathrm{ISHE}}(x, y)$ is generated in the presence of a temperature gradient. $\boldsymbol{E}_{\mathrm{ISHE}}(x, y)$ is, however, caused by a local spin current $\boldsymbol{J}_s(x, y)$. Hence the detection of $\boldsymbol{E}_{\mathrm{ISHE}}(x, y)$ not only allows us to electrically detect magnetic texture in a ferromagnetic insulator, but it even enables a spatial mapping of spin currents.

We first demonstrate magnetothermal domain imaging in a conductive ferromagnetic thin film via the anomalous Nernst effect. To this end, the setup depicted schematically in Fig. 1(a) is used [22]. It is operated at room temperature for all measurements discussed in this Letter. The light beam emitted by a laser diode is coupled into an optical fiber and focused onto the sample surface at position (x, y) by means of a scannable collimator. The laser-spot diameter was $d = 10\ \mu$m and the impinging laser power was $P = 7$ mW. Since the sample at least partially absorbs the laser light, its intensity and thus the energy deposited decrease as a function of depth. Hence, the energy absorption profile of the laser beam into the film thickness gives rise to a thermal gradient $\nabla_z T(x, y) \approx -1\ \mathrm{K}/\mu\mathrm{m}$ [22] perpendicular to the sample plane, laterally confined to a region around the position (x, y) of the laser spot [23]. This thermal gradient gives rise to a local electric field $\boldsymbol{E}_{\mathrm{ANE}}(x, y)$ [cf. Eq. (1)]. Temperature gradients within the sample plane are radially symmetric and their contributions to magnetothermal effects thus cancel out. We use a ferromagnetic Co_2FeAl thin film deposited on a MgO substrate [22]. The film is patterned into the Hall bar geometry shown in Fig. 1(a).

Figure 1(b) shows the dc voltage V_{ANE} recorded between the contacts 2 and 4 which are separated by approximately 460 μm. For each value of the in-plane magnetic field $\mu_0 H$ applied at an angle $\alpha = 90°$ to the $\boldsymbol{x}$ axis, we scanned the laser beam over the central Hall bar area in steps of 5 μm along $\boldsymbol{x}$ and $\boldsymbol{y}$ and recorded $V_{\mathrm{ANE}}(x, y)$. The small full rectangles indicate the location of the used electric contacts and the dashed rectangle depicts the region on the main Hall bar enclosed by these contacts. At $\mu_0 H = -15$ mT ($\boldsymbol{H} \parallel -\boldsymbol{y}$ as indicated by the solid arrow to the left) we observe a voltage $V_{\mathrm{ANE}} \approx -150$ mT in the Hall bar region independent of the laser-spot position (x, y). We attribute $V_{\mathrm{ANE}} \propto E_x$ to the anomalous Nernst effect defined in Eq. (1). At $\mu_0 H = -15$ mT the film is in magnetic saturation with $\boldsymbol{M} \parallel \boldsymbol{H}$ as shown later. Hence, no magnetic microstructure is present and $V_{\mathrm{ANE}}(x, y)$ does not change as a function of x and y. As the magnetic field magnitude is decreased to $\mu_0 H = -1.4$ mT, magnetic domain formation is evident from the V_{ANE} map and at $\mu_0 H = +0.2$ mT V_{ANE} vanishes in the major part of the Hall bar, indicating that $\boldsymbol{M}$ is oriented (anti)parallel to $\boldsymbol{x}$, such that $(\boldsymbol{M} \times \nabla T) \cdot \boldsymbol{x} = 0$. Note that Co_2FeAl has cubic magnetic anisotropy.

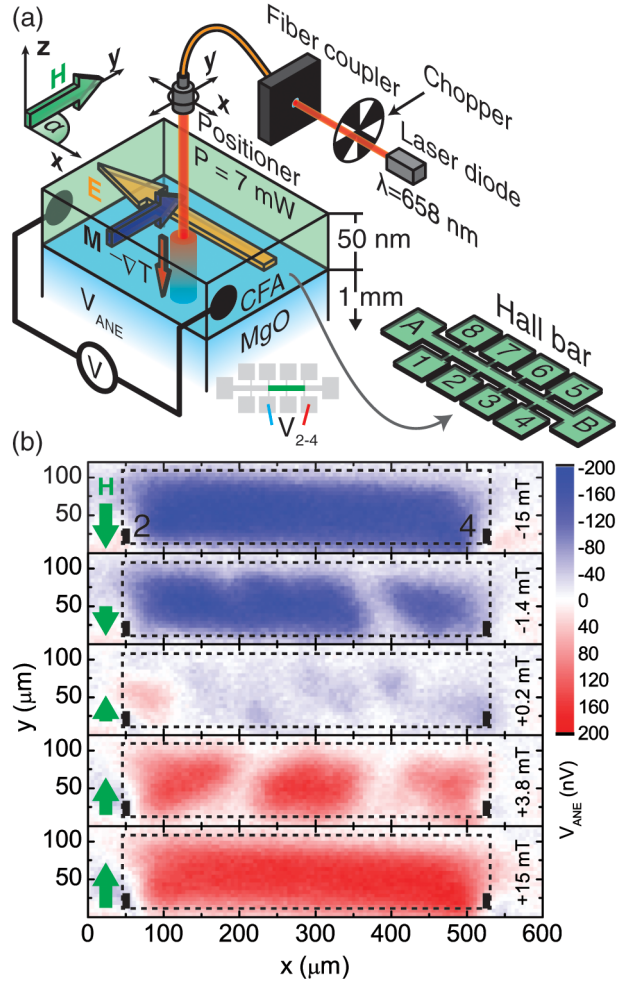

FIG. 1 (color online). (a) The scannable laser beam generates a local temperature gradient ∇T normal to the ferromagnetic thin film plane. The dc voltage V_{ANE} which arises due to the anomalous Nernst effect depends on the local magnetization $\boldsymbol{M}$ at the position (x, y) of the laser beam. All investigated samples are patterned into 80 μm wide and 900 μm long Hall bars with contacts labeled as sketched. (b) V_{ANE} determined between contacts 2 and 4 as a function of the laser-spot position (x, y) and the external magnetic field magnitude $\mu_0 H$ in a 50 nm thick Co_2FeAl (CFA) film.

As a consequence, the magnetic reversal proceeds via two 90° switches [24]. Upon increasing the external magnetic field to $\mu_0 H = +3.8$ mT, domains exhibiting $V_{\mathrm{ANE}} > 0$ become visible. In magnetic saturation at $\mu_0 H = +15$ mT, $V_{\mathrm{ANE}} \approx +150$ nV in the entire Hall bar region. The sign reversal of V_{ANE} with the reversal of the direction of $\boldsymbol{H}$ (and thus $\boldsymbol{M}$) is a clear indication that the observed V_{ANE} indeed is caused by a term $\nabla T \times \boldsymbol{M}$, which allows us to rule out all field-symmetric thermopower effects as the cause of the observed voltage. This is completely analogous to the Nernst signal in the mixed state of superconductors which changes sign upon switching the direction of the flux lines [25]. Furthermore, V_{ANE} is a local voltage as can be seen by the fact that $V_{\mathrm{ANE}}(x < 50\ \mu\mathrm{m}, y) = 0$ and

$V_{\mathrm{ANE}}(x > 550\ \mu\mathrm{m}, y) = 0$. For these x, the laser still impinges on the main Hall bar; it is, however, on either side of both contacts, rendering them at identical electrical potential [22]. Finally, the magnetic texture in Fig. 1(b) correlates well with the one recorded in magneto-optical Kerr effect experiments in the same sample [24], with large magnetic domains and domain walls predominantly aligned along the cubic [100] directions.

We now turn to the generation and detection of local spin currents via the longitudinal spin Seebeck effect in a ferromagnetic insulator exposed to magnetothermal landscapes. We employ a 10 nm thick $Y_3Fe_5O_{12}$ (YIG) film grown onto on a $Gd_3Ga_5O_{12}$ (GGG) substrate [22]. The YIG thin film was covered *in situ* by a 7 nm thick Pt film to take advantage of the inverse spin Hall effect for an all electrical detection of local spin currents. The YIG/Pt hybrid was patterned into the same Hall bar geometry as the Co_2FeAl sample. A schematic view of the sample and setup (which is identical to that used for the ANE measurements) is shown in Fig. 2(a). Upon application of $\nabla T \approx -9\ \mathrm{K}/\mu\mathrm{m}$ [22] along the hybrid normal via a laser beam with diameter $d = 10\ \mu\mathrm{m}$ and power $P = 9$ mW, the longitudinal SSE [12] yields a pure spin current $\boldsymbol{J}_s$ in the YIG film parallel to ∇T which can be detected by exploiting the inverse spin Hall effect in the Pt layer. Note that YIG is an electrical insulator, such that it does not show an anomalous Nernst effect. The Pt layer serves not only as a spin current detector but furthermore as an optical absorber of the laser light.

In Fig. 2(b) we present $V_{\mathrm{ISHE}} = V_{A-B}$ recorded with a scanning step size of 5 μm as a function of H. Figure 2(b) thus represents a map of magnetic domains in the ferromagnetic insulator YIG, detected by local electric fields in a Pt layer deposited on top. At $\mu_0 H = \pm 100$ mT (top and bottom panels) the YIG thin film is in a single domain state with $\boldsymbol{M} \parallel \boldsymbol{H}$. As $\boldsymbol{H}$ is applied along $\boldsymbol{y}$, we can observe $\boldsymbol{E}_{\mathrm{ISHE}}$ along $\boldsymbol{x}$ by probing V_{ISHE} [cf. Eq. (2)]. As we used contacts A and B for recording V_{ISHE}, the laser-spot position is located between the used contacts for all values of x in Fig. 2(b). For all values of y where the laser impinges on the 80 μm wide Hall bar, $V_{\mathrm{ISHE}} = +640$ nV in magnetic saturation with $\mu_0 H = +100$ mT. Magnetic texture can be observed during the magnetic field sweep in the images recorded with $\mu_0 H = +8.2$ mT to $\mu_0 H = -12.4$ mT (middle panels). As our YIG (111) films show only very small magnetic anisotropy in the film plane the magnetic domain pattern is more complex than that observed in Co_2FeAl and the smallest discernible feature is limited by the scanning step size [22]. We note that—while our YIG thin films are electrically insulating—magnetotransport measurements on our YIG/Pt samples showed an anisotropic magnetoresistance $\Delta R/R \approx 7 \times 10^{-4}$ [22] attributed to induced magnetic moments in the Pt thin film close to the interface [26]. An interpretation of V_{ISHE} on the basis of Nernst effects in Pt would require implausible

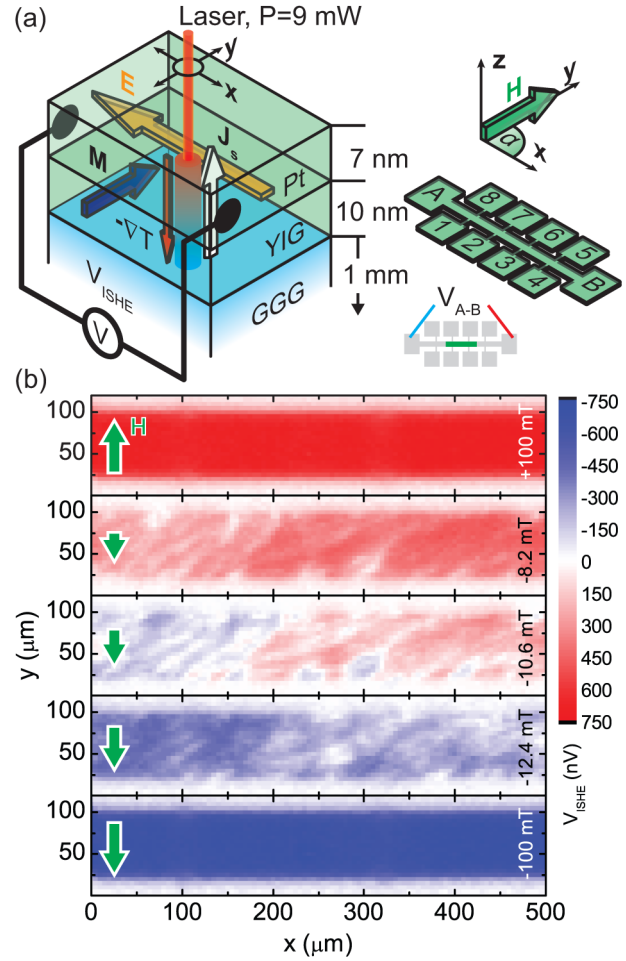

FIG. 2 (color online). (a) Sample schematics of GGG/YIG/Pt sample. The spin Seebeck effect yields a pure, local spin current $\boldsymbol{J}_s$ along ∇T in YIG. $\boldsymbol{J}_s$ depends on the local magnetization $\boldsymbol{M}(x, y)$ and is detected using the inverse spin Hall effect in Pt, which gives rise to a dc voltage V_{ISHE}. (b) V_{ISHE} determined between contacts A and B as a function of the laser-spot position (x, y) and the external magnetic field magnitude $\mu_0 H$ applied along $\boldsymbol{y}$ in a 10 nm YIG/7 nm Pt hybrid sample.

Nernst coefficients [22]. We thus attribute the magnetothermal voltage observed to the longitudinal SSE.

To quantitatively compare our spatially resolved magnetothermal voltages with the known integral properties, we average V_{ANE} and V_{ISHE} within the illuminated regions. Such integral measurements are presented in Fig. 3, where the insets depict the regions of interest used for averaging. In Fig. 3(a), V_{ANE} in Co_2FeAl is shown as a function of the external magnetic field magnitude $\mu_0 H$ for three different orientations α of the external magnetic field in the plane of the film. For $\alpha = 90°$ (circles), we observe a double step switching behavior indicating cubic magnetic anisotropy. For large H applied at $\alpha = 90°$, $\boldsymbol{M}$ is oriented perpendicular to the main Hall bar. Hence, the generated electric field $\boldsymbol{E}$ is parallel to the main Hall bar and can be probed by the potential difference between the used contacts. For

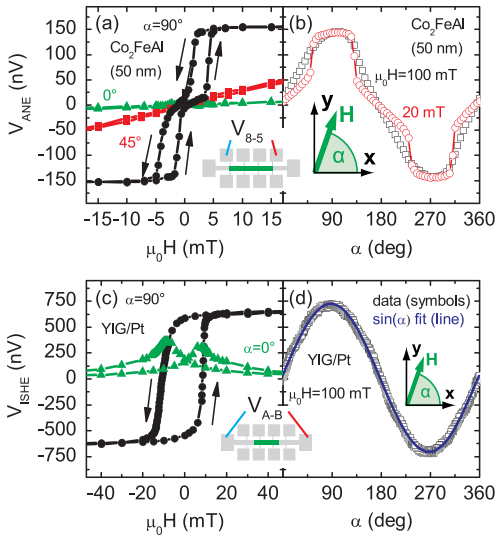

FIG. 3 (color online). (a) Averaged V_{ANE} in Co_2FeAl using the region of interest and contacts shown in the inset as a function of $\mu_0 H$ for $\alpha \in \{0°, 45°, 90°\}$ (triangles, squares, circles). (b) Sinelike angular dependency of V_{ANE} on α at $\mu_0 H = 100$ mT (squares). At $\mu_0 H = 20$ mT (circles), the abrupt $\boldsymbol{M}$ switching across the magnetically hard axes (45° and 135°) becomes visible as steps in V_{ANE}. (c) Averaged V_{ISHE} in YIG/Pt within the main Hall bar region as a function of $\mu_0 H$ for $\alpha \in \{0°, 90°\}$ (triangles, circles). (d) V_{ISHE} as a function of α (symbols). The solid curve is a fit to $\sin(\alpha)$ showing excellent agreement with data.

$\alpha = 45°$, V_{ANE} is smaller, as only the projection of $\boldsymbol{E}$ on the $\boldsymbol{x}$ direction is probed. Furthermore, at this value of α, $\boldsymbol{H}$ is oriented along a magnetically hard axis of the Co_2FeAl film, so hysteresis is minimal. Finally, for $\alpha = 0°$, V_{ANE} vanishes because $\boldsymbol{E}$ is generated along the $\boldsymbol{y}$ direction and thus cannot be detected by voltage contacts aligned along the $\boldsymbol{x}$ direction. The evolution of V_{ANE} as a function of $\boldsymbol{H}$ orientation is shown in more detail in Fig. 3(b), where V_{ANE} data recorded during a rotation of $\mu_0 H = 100$ mT within the film plane are depicted (squares). A dependence $V_{\mathrm{ANE}} \propto \sin(\alpha)$ is observed in agreement with the cross product found in Eq. (1). In an analogous experiment with $\mu_0 H = 20$ mT, a similar behavior is found (circles). However, at the four magnetically hard axes along 45°, 135°, 225°, and 315°, the magnetization switches abruptly, as is evident from the steps in V_{ANE} at these orientations. This shows that the anomalous Nernst effect measurements can be used to probe magnetic anisotropy in the same fashion as in angular dependent magnetoresistance (ADMR) measurements [27], but with spatial resolution.

Figure 3(c) shows $V_{A-B} = V_{\mathrm{ISHE}} \propto E_{\mathrm{ISHE}}$ obtained in the YIG/Pt bilayer as a function of the external magnetic field for $\alpha = 90°$ (circles) and $\alpha = 0°$ (triangles). As expected from Eq. (2), and following the same line of arguments as for V_{ANE}, we observe an antisymmetric V_{ISHE} versus H behavior for $\alpha = 90°$ while for $\alpha = 0°$, V_{ISHE} vanishes for large values of H. In Fig. 3(d) we present V_{ISHE} data as a function of α (symbols) recorded with $\mu_0 H = 100$ mT together with a fit to $\sin(\alpha)$ (line). The excellent agreement between fit and data corroborates the cross product in Eq. (2). Thus, by exploiting the SSE it is possible to perform spatially resolved ADMR-like measurements in magnetic insulators.

Upon calculating the temperature gradient ∇T evoked by the laser heating, we can quantify the anomalous Nernst coefficient N and the spin Seebeck coefficient S of the investigated samples. For Co_2FeAl, such a quantitative evaluation is not straightforward, since neither the optical properties nor the Nernst coefficient have been reported. We thus performed further V_{ANE} measurements in a Ni thin film sample [22]. For Ni, we calculated $\nabla T = -1.4$ K/μm [22] for $P = 9$ mW and $d = 10$ μm. Using a saturation magnetization $M_s = 370$ kA/m obtained by SQUID magnetometry [28] and the experimentally measured $E = 87$ mV/m [22], we obtain the Nernst coefficient $N_{\mathrm{Ni}} \approx 1.3 \times 10^{-7}$ V/KT, which is lower than values $N_{\mathrm{Ni}} \approx 5 \times 10^{-7}$ V/KT found for bulk Ni [29] at room temperature. A comparable reduction of a caloritronic property with respect to bulk material was recently reported for the Seebeck coefficient in Ni thin films [30]. Assuming comparable optical and thermal properties for Co_2FeAl (CFA) and thus $\nabla T = -1.4$ K/μm in a 80 nm thick Co_2FeAl sample with $M_s = 1050$ kA/m obtained by SQUID magnetometry, we estimate $N_{\mathrm{CFA}} \approx 9.5 \times 10^{-8}$ V/KT. We now turn to the longitudinal spin Seebeck coefficient of the YIG/Pt bilayer. Using a calculated mean temperature gradient of $\nabla T = -8.7$ K/μm [22] at $P = 9$ mW and $d = 10$ μm in the YIG thin film, we obtain a spin Seebeck coefficient $S = 5.9 \times 10^{-8}$ V/K, compared to $S = 1 \times 10^{-7}$ V/K found in [12]. We assume that the small difference in S is due to different interfaces of Pt and YIG as well as different Pt thicknesses. Taken together, the above results show that, by exploiting the longitudinal SSE in a magnetothermal landscape, a determination of the magnetic microstructure by means of an integral voltage measurement is possible even in a ferromagnetic insulator. Furthermore, the spatially resolved SSE and ANE open an avenue for the local generation of pure spin or bipolar charge currents with magnetically selectable (spin) polarization.

In conclusion, our results show that spatially resolved spin caloritronics are a viable path for the use of heat landscapes in spintronic applications. In conductive ferromagnetic thin films, we demonstrated that a spatially confined thermal gradient allows for the generation of a local, magnetically controllable, electric field via the anomalous Nernst effect. Our results furthermore suggest that in magnetic-insulator–normal-metal hybrids, a spatially confined temperature gradient gives rise to local, pure spin currents with magnetically selectable spin polarization due to the longitudinal spin Seebeck effect. This opens exciting

perspectives for the generation, the study, and the use of local pure spin currents.

Financial support from the DFG via SPP 1538 "Spin Caloric Transport," Project No. GO 944/4-1, and the German Excellence Initiative via the "Nanosystems Initiative Munich" (NIM) is gratefully acknowledged.

*goennenwein@wmi.badw.de

[1] W. Nernst, Ann. Phys. (Leipzig) **267**, 760 (1887).
[2] T. C. Harmann and J. M. Honig, *Thermoelectric and Thermomagnetic Effects and Applications* (McGraw-Hill, New York, 1967).
[3] R. P. Vasil'eva and B. Akmuradov, Russ. Phys. J. **15**, 814 (1972).
[4] T. Miyasato, N. Abe, T. Fujii, A. Asamitsu, S. Onoda, Y. Onose, N. Nagaosa, and Y. Tokura, Phys. Rev. Lett. **99**, 086602 (2007).
[5] R. Suryanarayanan, V. Gasumyants, and N. Ageev, Phys. Rev. B **59**, R9019 (1999).
[6] W.-L. Lee, S. Watauchi, V. L. Miller, R. J. Cava, and N. P. Ong, Phys. Rev. Lett. **93**, 226601 (2004).
[7] N. Hanasaki, K. Sano, Y. Onose, T. Ohtsuka, S. Iguchi, I. Kézsmárki, S. Miyasaka, S. Onoda, N. Nagaosa, and Y. Tokura, Phys. Rev. Lett. **100**, 106601 (2008).
[8] Y. Pu, D. Chiba, F. Matsukura, H. Ohno, and J. Shi, Phys. Rev. Lett. **101**, 117208 (2008).
[9] K. Uchida, S. Takahashi, K. Harii, J. Ieda, W. Koshibae, K. Ando, S. Maekawa, and E. Saitoh, Nature (London) **455**, 778 (2008).
[10] J. E. Hirsch, Phys. Rev. Lett. **83**, 1834 (1999).
[11] E. Saitoh, M. Ueda, H. Miyajima, and G. Tatara, Appl. Phys. Lett. **88**, 182509 (2006).
[12] K. Uchida, H. Adachi, T. Ota, H. Nakayama, S. Maekawa, and E. Saitoh, Appl. Phys. Lett. **97**, 172505 (2010).
[13] S. Bosu, Y. Sakuraba, K. Uchida, K. Saito, T. Ota, E. Saitoh, and K. Takanashi, Phys. Rev. B **83**, 224401 (2011).
[14] C. M. Jaworski, J. Yang, S. Mack, D. D. Awschalom, J. P. Heremans, and R. C. Myers, Nature Mater. **9**, 898 (2010).
[15] K. Uchida, J. Xiao, H. Adachi, J. Ohe, S. Takahashi, J. Ieda, T. Ota, Y. Kajiwara, H. Umezawa, H. Kawai, G. E. W. Bauer, S. Maekawa, and E. Saitoh, Nature Mater. **9**, 894 (2010).
[16] L. Gravier, S. Serrano-Guisan, and J.-P. Ansermet, J. Appl. Phys. **97**, 10C501 (2005).
[17] L. Gravier, S. Serrano-Guisan, F. Reuse, and J.-P. Ansermet, Phys. Rev. B **73**, 024419 (2006).
[18] J. C. Slonczewski, Phys. Rev. B **82**, 054403 (2010).
[19] H. Yu, S. Granville, D. P. Yu, and J.-P. Ansermet, Phys. Rev. Lett. **104**, 146601 (2010).
[20] A. Slachter, F. L. Bakker, J. Adam, and B. J. van Wees, Nature Phys. **6**, 879 (2010).
[21] J.-C. Le Breton, S. Sharma, H. Saito, S. Yuasa, and R. Jansen, Nature (London) **475**, 82 (2011).
[22] See Supplemental Material at http://link.aps.org/supplemental/10.1103/PhysRevLett.108.106602 for details.
[23] M. Reichling and H. Grönbeck, J. Appl. Phys. **75**, 1914 (1994).
[24] M. Weiler, F. D. Czeschka, A. Brandlmaier, I.-M. Imort, G. Reiss, A. Thomas, G. Woltersdorf, R. Gross, and S. T. B. Goennenwein, Appl. Phys. Lett. **98**, 042501 (2011).
[25] H.-C. Ri, R. Gross, F. Gollnik, A. Beck, R. P. Huebener, P. Wagner, and H. Adrian, Phys. Rev. B **50**, 3312 (1994).
[26] F. Wilhelm, P. Poulopoulos, G. Ceballos, H. Wende, K. Baberschke, P. Srivastava, D. Benea, H. Ebert, M. Angelakeris, N. K. Flevaris, D. Niarchos, A. Rogalev, and N. B. Brookes, Phys. Rev. Lett. **85**, 413 (2000).
[27] W. Limmer, M. Glunk, J. Daeubler, T. Hummel, W. Schoch, R. Sauer, C. Bihler, H. Huebl, M. S. Brandt, and S. T. B. Goennenwein, Phys. Rev. B **74**, 205205 (2006).
[28] M. Weiler, A. Brandlmaier, S. Geprägs, M. Althammer, M. Opel, C. Bihler, H. Huebl, M. S. Brandt, R. Gross, and S. T. B. Goennenwein, New J. Phys. **11**, 013021 (2009).
[29] A. W. Smith, Phys. Rev. **33**, 295 (1911).
[30] A. D. Avery, R. Sultan, D. Bassett, D. Wei, and B. L. Zink, Phys. Rev. B **83**, 100401 (2011).